Section S1: Contributions to interannual variability of simulated CO

The improved method for CO-only simulation described in this work requires first completing a run of the full chemistry simulation to save mean CO chemical production rates (P(CO)). In Section 2.2.2, we suggest that the P(CO) fields could be saved while benchmarking the GEOS-Chem standard full chemistry simulation for public release, and that for many applications use of a single year of P(CO) fields would be sufficient.

To evaluate this claim, we performed a set of sensitivity simulations designed to quantify the contribution of P(CO) to overall interannual variability. We compared three simulations: (1) a simulation with 2009 meteorology/emissions and 2009 P(CO); (2) a simulation with 2009 meteorology/emissions and 2010 P(CO); and (3) a simulation with 2010 meteorology/emissions and 2010 P(CO). The difference between (3) and (1) gives the overall CO variability between the two years. The contribution caused by the interannual variability of P(CO) is the difference between (2) and (1), while the contribution caused by the interannual variability of other factors (meteorology, emissions) is the difference between (3) and (2).

Figure S2 shows the results from these comparisons for July (other months are similar). At both the surface and 500 hPa, the interannual variability of P(CO) makes only a minor contribution (<7%) to the overall variability. Other factors (meteorology, emissions) clearly dominate the simulated year-to-year differences. The impacts of large, yearly-varying biomass burning events can clearly be seen over Indonesia (intense fires in 2009, no fires in 2010), central Canada (intense fires in 2010, no fires in 2009), and western Russia (intense fires in 2010, weak fires in 2009). These year-to-year differences in biomass burning drive large interannual variability in total CO (Fig. S2a), but the majority of this is driven by the variability in primary emissions (Fig. S2b) rather than the variability in P(CO) (Fig. S2c). We performed the same test for 2011 and found the same result.

We also evaluated the impacts for CO source attribution using the same simulations (2009, 2009 meteorology/emissions with 2010 P(CO), and 2010). For each simulation, we calculated the contributions from different source types (primary fossil anthropogenic, primary biomass burning, and NMVOC oxidation) and source regions (for NMVOC oxidation) at the three Australasian TCCON sites described in Sect. 5 of the main text. Figure S3 shows the results for February, when there were extremely large fires in southeast Australia in 2009 but none in 2010, and October, when there were much larger fires in northern Australia in 2009 than 2010 and larger fires in southern Africa in 2010 than in 2009.

Figure S3 shows that meteorology and primary emissions generally dominate the interannual variability in source contributions. The largest year-to-year differences at all sites come from primary biomass burning emissions. Interannual variability in P(CO) can also drive small differences in CO from NMVOC oxidation, particularly near large and variable emission sources. This is most evident at Darwin in October, when the large decrease in Australian biomass burning emissions from 2009-2010 was associated with a decrease in P(CO) from Australian NMVOC oxidation as well. Downwind of sources, these impacts become negligible. For example, the larger burning in southern Africa in 2010 than 2009 can clearly be seen in the primary emissions contribution at Wollongong and Lauder, but the changes in the African NMVOC source are minimal at both sites.

These tests suggest that use of a single year of P(CO) fields will be appropriate for many applications of the CO-only simulation. The errors introduced by this

approach are significantly smaller than the difference between the base and improved methods described here. The exception would be any studies specifically focused on secondary CO (for example, evaluating impacts of using different biogenic emission inventories), or specifically evaluating source attribution near major and variable primary emission sources. In these cases, it would be necessary for an interested user to re-run the full chemistry simulation and save *P*(CO) for each scenario to be evaluated.

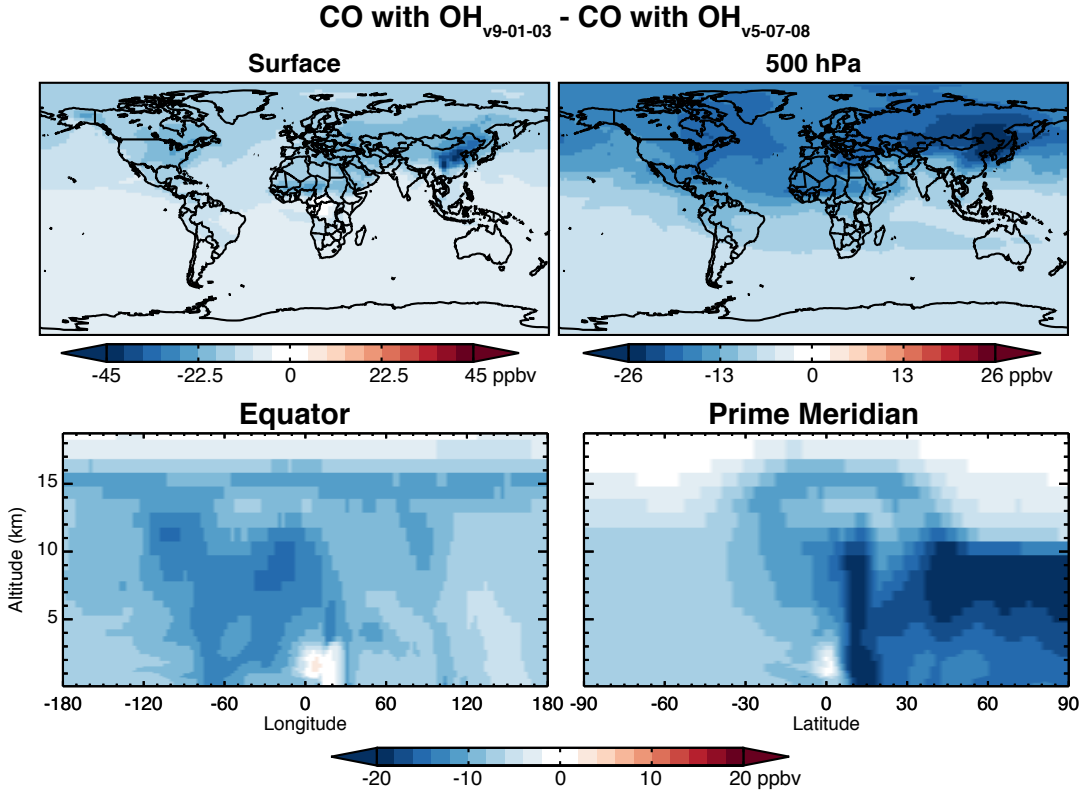

Fig. S1. Decrease in CO mixing ratio introduced by updating the OH concentration fields from v5-07-08 to v9-01-03. The two simulations are otherwise identical and use the original CO-only formulation. The "CO with $OH_{v9\text{-}01\text{-}03}$" simulation is the same as the base simulation shown elsewhere. All plots are for July 2009, but results are similar for others months/years.

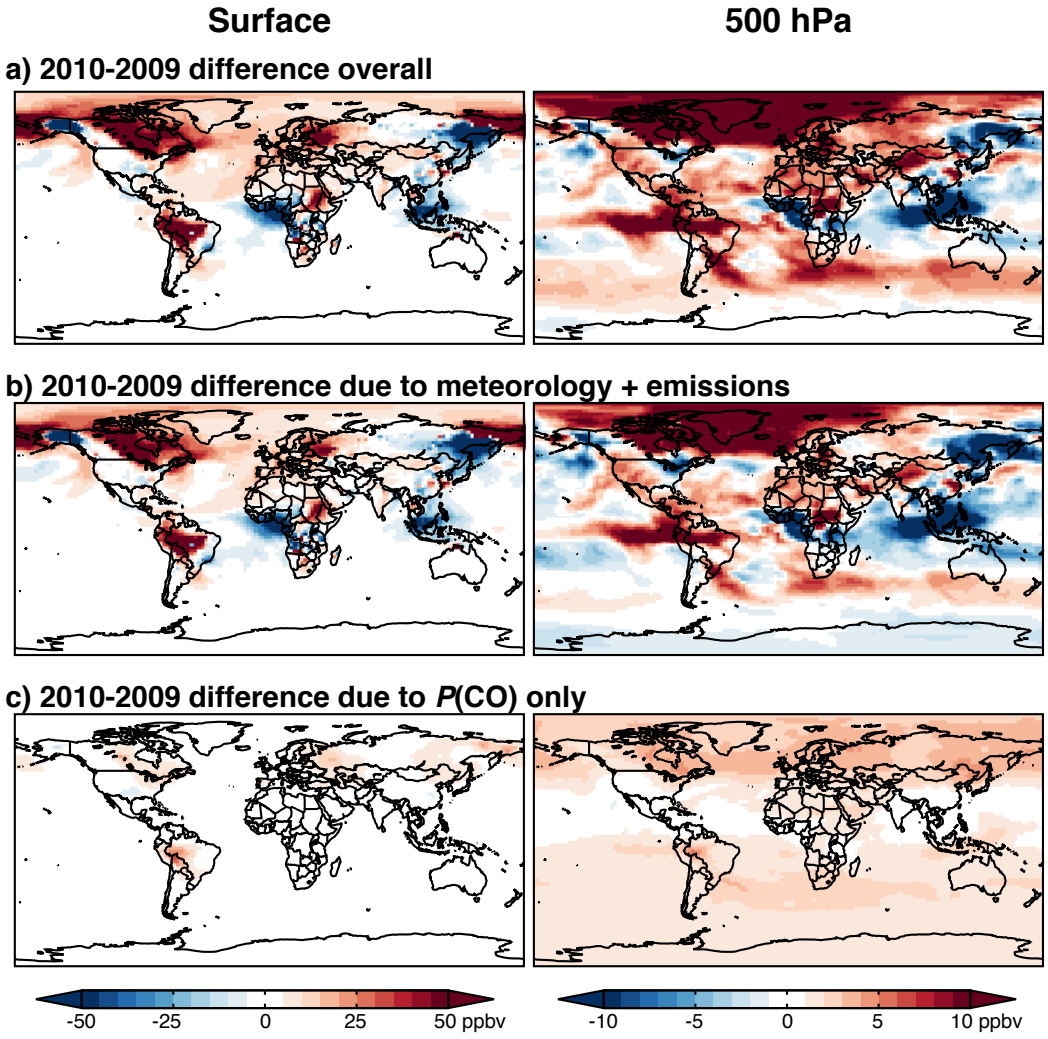

Fig. S2. Contributions to year-to-year variability in simulated CO in the improved simulation. (a) Overall difference between a simulation for the year 2010 and a simulation for the year 2009. (b) Contribution to the difference from all factors except *P*(CO), derived by comparing a simulation for the year 2010 to a simulation for the year 2009 but using 2010 *P*(CO). (c) Contribution to the difference from *P*(CO) only, derived by comparing a simulation for the year 2009 to a simulation for the year 2009 but using 2010 *P*(CO). All plots are for July, but results are similar for others months.

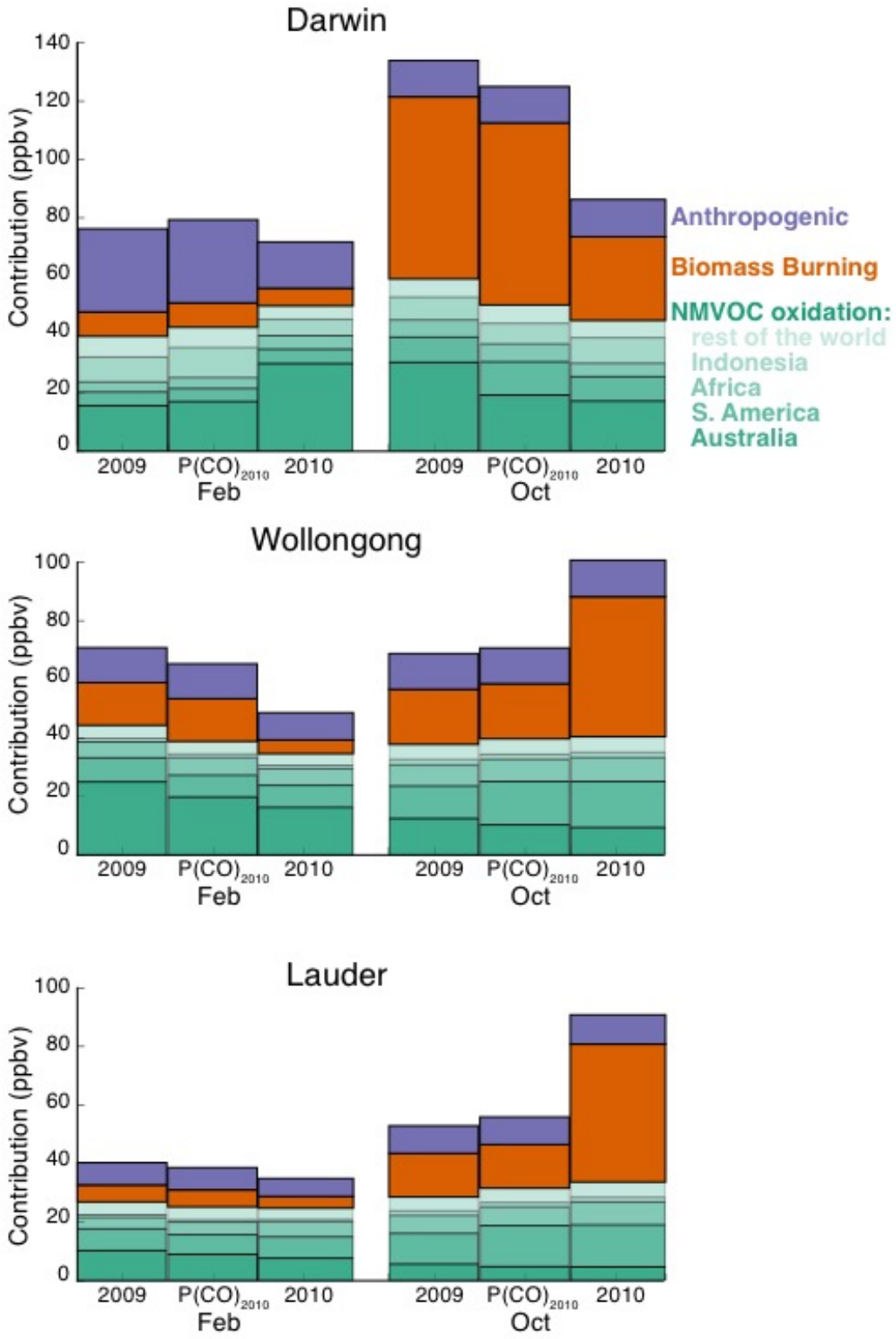

Fig. S3. Year-to-year variability and drivers in simulated CO source attribution at the Australasian TCCON sites in February and October (see text for site details). The figure compares CO simulated using 2009 inputs (left bars), 2009 meteorology and primary emissions with 2010 secondary production (middle bars), and 2010 inputs (right bars). Differences between the left and middle bars are driven by *P*(CO), while differences between middle and right bars are driven by meteorology and emissions. Colors show contributions from different source types and regions, as described in the caption to Fig. 7 in the main text.

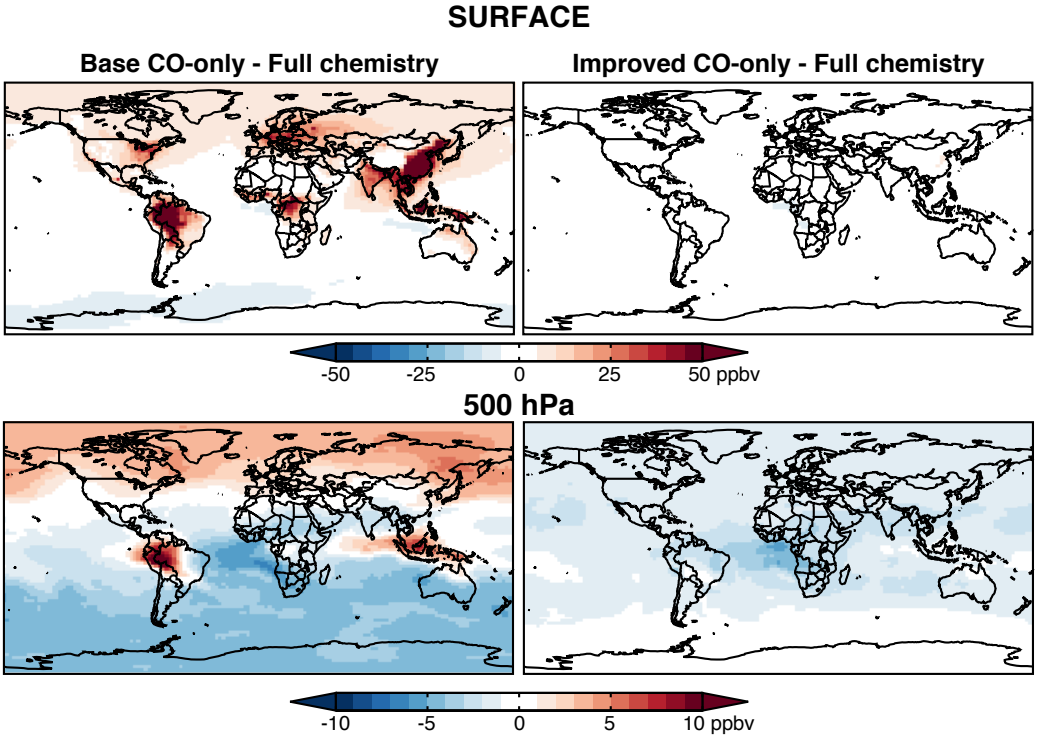

Fig. S4. Same as Figure 1, but for January 2009 to highlight seasonal variability. For other months and years, see full benchmark results included in the supplement.

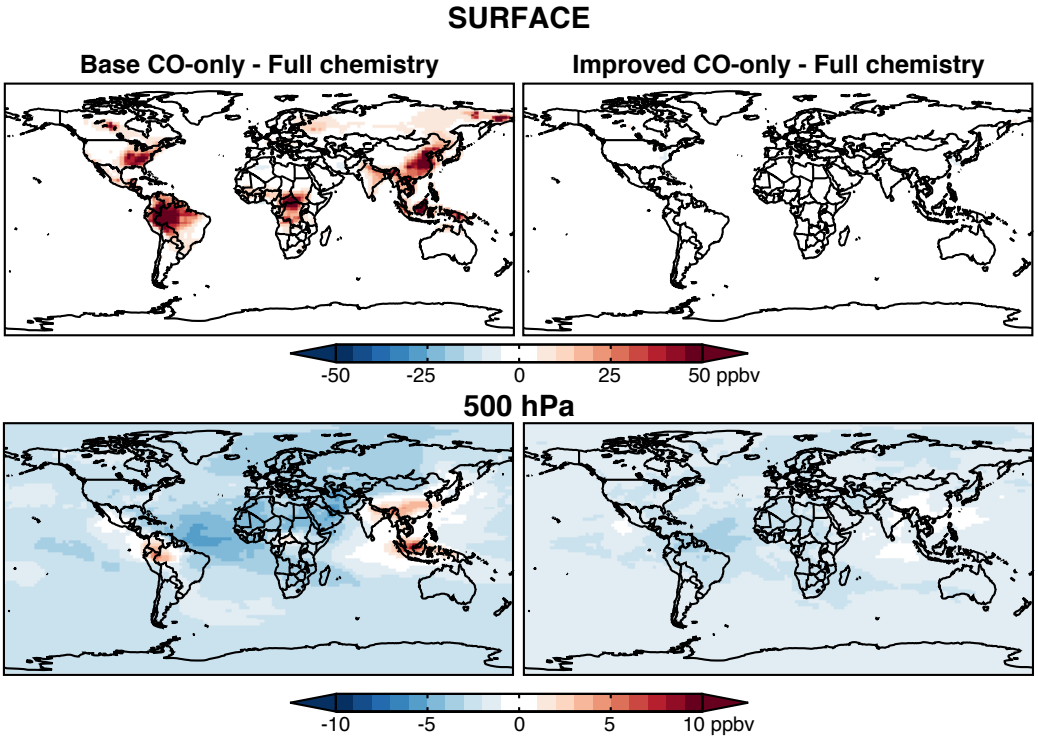

Fig. S5. Same as Figure 1, but for July 2010 to highlight interannual variability. For other months and years, see full benchmark results included in the supplement.

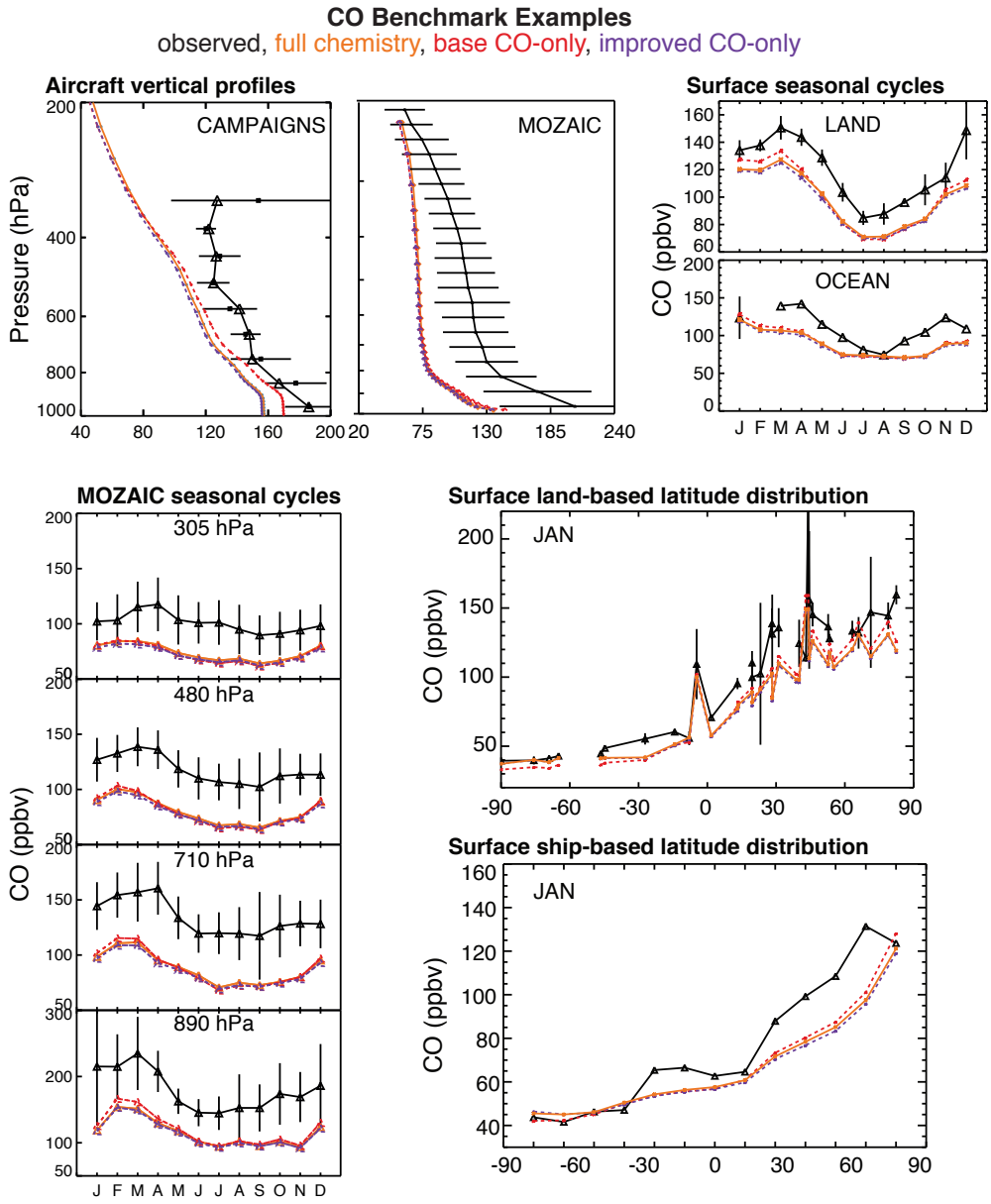

Fig. S6. Representative examples of the plot types produced by the GEOS-Chem CO benchmark evaluation. Plot types include: aircraft vertical profiles (top left), both from short-term campaigns and from MOZAIC data separated by seasons; aircraft seasonal cycles (bottom left) from MOZAIC data separated by altitude; surface seasonal cycles (top right) from NOAA GMD land and ocean sites; and surface latitude distributions (bottom right) from a subset of land-based and ship-based NOAA GMD sites. For the full set of benchmark plots, included in the supplement.

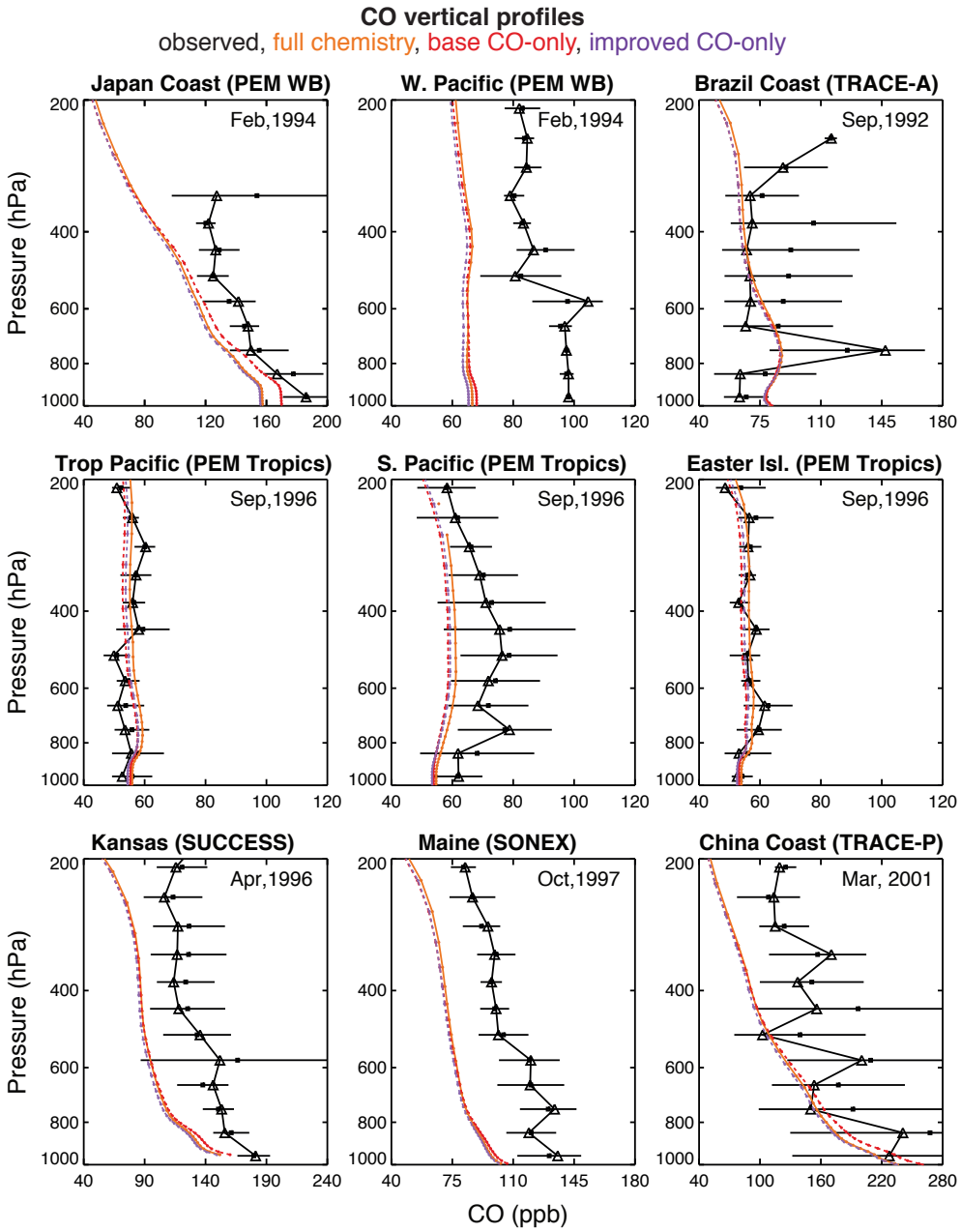

Fig. S7. Same as Figure 5, but for additional aircraft data available in the GEOS-Chem benchmark. Additional campaigns and regions can be seen in the full benchmarks included in the supplement.

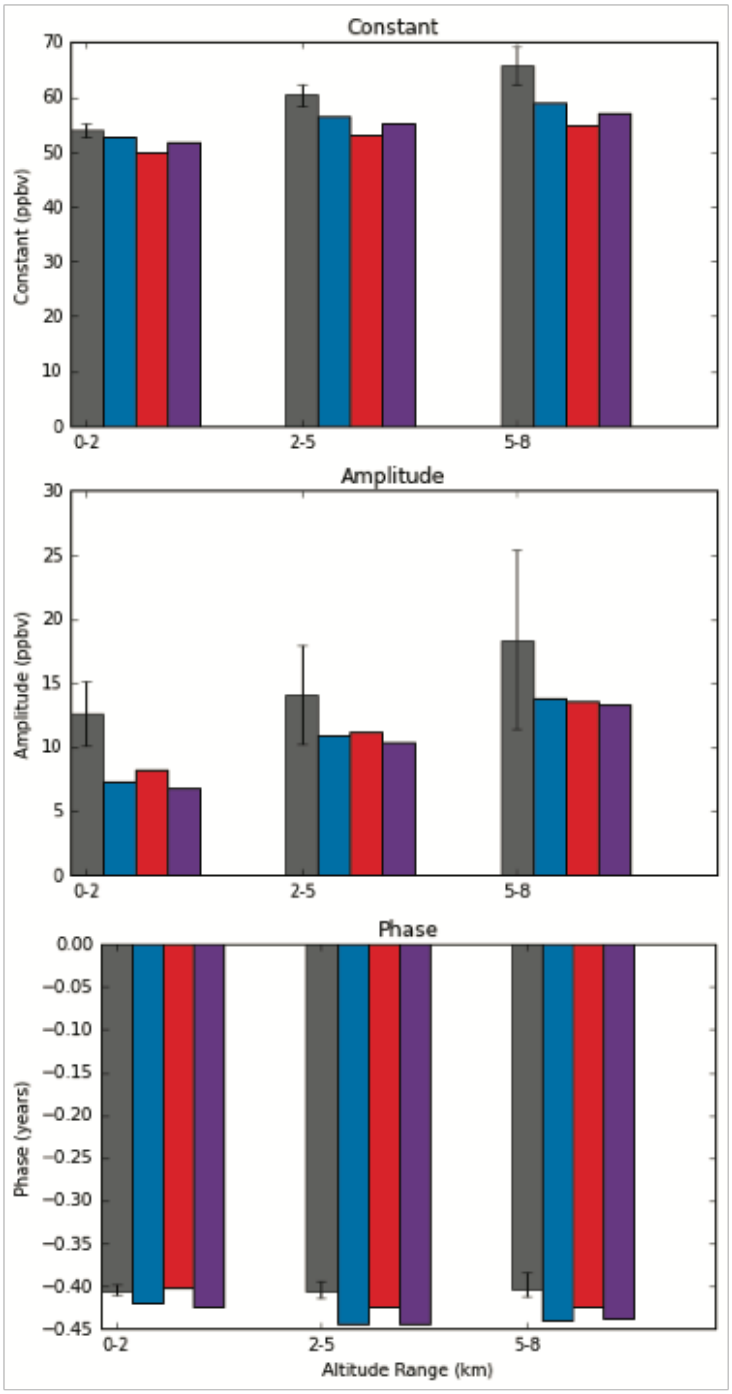

Fig. S8. Parameters for a single harmonic fit describing the shape of the seasonal cycle of carbon monoxide in the remote southern hemisphere (in/around Cape Grim, Australia) in different altitude bins. Grey bars represent the fit to the observations (including 95% confidence intervals) and coloured bars represent the GEOS-Chem full chemistry (blue), base CO-only (red) and updated CO-only (purple) simulations. For full details of the method and motivation of the fit, see Fisher et al. (2015).

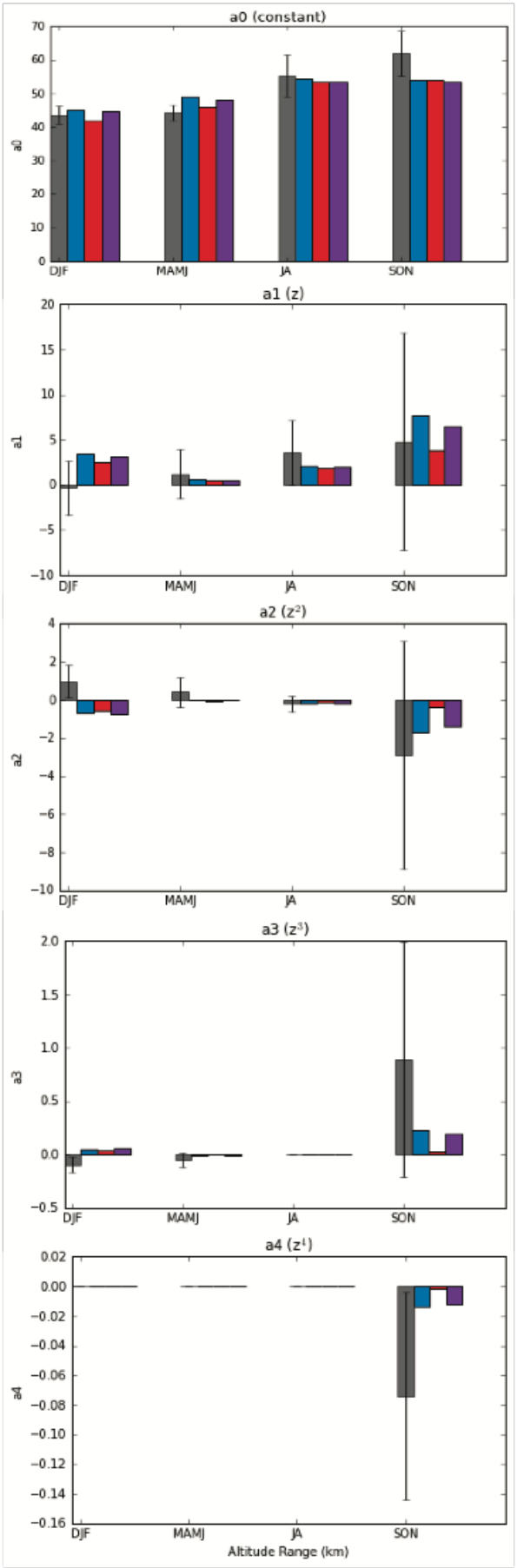

Fig. S9. Polynomial terms representing the shape of the vertical profile of carbon monoxide in the remote southern hemisphere (in/around Cape Grim, Australia) in different seasons. Grey bars represent the fit to the observations (including 95% confidence intervals) and coloured bars represent the GEOS-Chem full chemistry (blue), base CO-only (red) and updated CO-only (purple) simulations. For full details of the method and motivation of the fit, see Fisher et al. (2015).